EUROPEAN ORGANIZATION FOR NUCLEAR RESEARCH

CERN/EP 85-30
5 March 1985

A DIQUARK SCATTERING MODEL FOR HIGH p_T PROTON PRODUCTION IN pp COLLISIONS AT THE ISR

Ames-Bologna-CERN-Dortmund-Heidelberg-Warsaw Collaboration

A. Breakstone[1(+)], H.B. Crawley[1], G.M. Dallavalle[5], K. Doroba[6], D. Drijard[3], F. Fabbri[3], A. Firestone[1], H.G. Fischer[3], H. Frehse[3(*)], W. Geist[3(**)], G. Giacomelli[2], R. Gokieli[6], M. Gorbics[1], P. Hanke[5], M. Heiden[3(**)], W. Herr[5], E.E. Kluge[5], J.W. Lamsa[1], T. Lohse[4], R. Mankel[4], W.T. Meyer[1], T. Nakada[3(***)], M. Panter[3], A. Putzer[5], K. Rauschnabel[4], B. Rensch[5], F. Rimondi[2], M. Schmelling[4], G. Siroli[2], R. Sosnowski[6], M. Szczekowski[3], O. Ullaland[3] and D. Wegener[4]

1 Ames Laboratory and Physics Department, Iowa State University, Ames, USA.

2 Istituto di Fisica dell'Università and INFN, Bologna, Italy.

3 CERN, European Organization for Nuclear Research, Geneva, Switzerland.

4 Institut für Physik der Universität Dortmund, Germany.

5 Institut für Hochenergiephysik der Universität Heidelberg, Germany.

6 University and Institute for Nuclear Studies, Warsaw, Poland.

Submitted to Zeitschrift für Physik C

(+) Now at Dept. of Physics, University of Hawaii, USA.

(*) Now at CDC, Zurich, Switzerland.

(**) Now at LBL, Berkeley, California, USA.

(***) Now at SIN, Villigen, Switzerland.

EP/2702P/WG/mk

ABSTRACT

The relative yield of high transverse momentum protons measured in pp interactions at the CERN ISR is calculated in the framework of simple parton models. Whereas models based exclusively on quark and gluon scattering fail to describe the data, the hypothesis of diquark scattering provides a quantitative understanding of the measured dependences on transverse momentum, polar angle, and centre-of-mass energy. Different assumptions on diquark structure functions are tested.

1. INTRODUCTION

Recently we reported on the measurement of baryon production at high transverse momenta ($p_T \geq 3$–4 GeV/c) and intermediate polar angles θ of 10°, 20° and 45° in pp collisions at a centre-of-mass energy $\sqrt{s} = 62$ GeV [1]. From a qualitative discussion it was concluded that the differential relative proton yields are hardly understandable in the framework of lowest order hard quark and gluon scattering and common fragmentation schemes. It will be shown in the following that the data can, however, be well described in the framework of hard scattering of diquarks. These are hypothetical bound states of two quarks, which are not calculable in perturbative QCD.

The data presented in ref. [1] are summarized in sect. 2 and supplemented by a measurement of the $\sqrt{s}$ dependence. The model is described in sect. 3 and compared to the data in sect. 4.

2. THE DATA

The measured p_T dependence of the ratios $\sigma(p)/\sigma(K^+)$, $\sigma(\bar{p})/\sigma(K^-)$, $\sigma(p)/\sigma(\pi^+)$, and $\sigma(\bar{p})/\sigma(\pi^-)$ is shown in fig. 1 [1]. The θ dependence of the proton and antiproton fractions ($R(p) = \sigma(p)/\sigma(\text{all pos.})$ and $R(\bar{p}) = \sigma(\bar{p})/\sigma(\text{all neg.})$) at fixed p_T (~ 3.8 GeV/c for R(p) and ~ 4.4 GeV/c for $R(\bar{p})$) is presented in fig. 2. The strong p_T and θ dependences of R(p) and the large difference when compared to $R(\bar{p})$ are difficult to explain by standard parton models. If protons and positive mesons were produced by the same scattering mechanism, R(p) would be constant in all kinematic variables (as is the case, for example, for the ratio $\sigma(K^+)/\sigma(\pi^+)$ [2]) and would be comparable in magnitude to $R(\bar{p})$. This is reflected by the model predictions from sect. 3 indicated by the dotted lines in figs 1 and 2.

For $\theta \sim 45°$ the ratios $\sigma(p)/\sigma(\pi^+)$ at $\sqrt{s} = 31$ GeV and $\sqrt{s} = 44$ GeV were estimated from the measured ratios $(\sigma(p)+\sigma(K^+))/\sigma(\pi^+)$ [2,3] (protons were not separated from kaons at $\sqrt{s} = 31$ and 44 GeV) using the fact that $\sigma(K^+)/\sigma(\pi^+) \sim 0.45$ (systematic uncertainty $\pm$ 0.05) independent of

p_T (for $p_T \gtrsim 3$ GeV/c) and of $\sqrt{s}$ [2]. These data are shown in fig. 3 for a fixed value of the scaling variable $x_T = 2p_T/\sqrt{s} = 0.15$. Data points obtained at lower energies at $\theta \sim 90°$ [4] are also shown for the same value of x_T. The ratio $\sigma(p)/\sigma(\pi^+)$ is seen to decrease with increasing $\sqrt{s}$ at this fixed value of x_T. This observation also disagrees with the naive expectations based on quark and gluon scattering (dotted line in fig. 3).

It is the availability of these new data covering a wide kinematical range and the marked deviations from these naive expectations that motivated the present investigation of diquark scattering.

It should also be mentioned that an unexpectedly large proton yield, possibly of the same origin, was found in deep inelastic lepton nucleon interactions by the European Muon Collaboration (EMC) [5]. In fig. 4 the proton and antiproton fractions in the current jets are shown for Bjorken $x > 0.2$ as functions of the fractional jet momentum z. Studies based on Monte-Carlo simulation have shown [6] that a high p_T particle at $\theta \sim 45°$ and $p_T \sim 4$ GeV/c originates from a scattered parton at $\langle x \rangle \sim 0.3$ and takes about 70–75% of the jet momentum [7]. Hence in this kinematic region the high p_T particle from the trigger jet is comparable to a high z particle in the current jet in lepton–nucleon interactions. The fractions R(p) and $R(\bar{p})$ for $p_T \sim 4$ GeV/c and $\theta \sim 45°$ are therefore also shown in fig. 4 at a fractional momentum $z \sim 0.75$. The similarity with the EMC data is remarkable. Fig. 4 also shows a theoretical prediction of the EMC group based on the LUND fragmentation model [8]. It fails to reproduce the large difference between the p and $\bar{p}$ fractions.

3. DESCRIPTION OF THE MODELS

In the following we confront quantitative model predictions with our data. The basic approach was suggested in ref. [9]. However, more refined calculations are performed over a larger kinematical range. We show that the proton fractions may be understood on the basis of the

scattering of bound diquark systems inside the incident protons. As in [9] scalar ud systems are assumed to dominate; uu states are neglected. Detailed calculations require a fragmentation scheme which is capable of describing diquark hadronization and a quantitative formulation for the proton structure in terms of quark, gluon and diquark structure functions. In this section the ingredients of our models will be briefly described. Further details on the treatment of quarks and gluons are given in ref. [6].

3.1 Fragmentation functions

In order to calculate inclusive cross sections for high p_T single particle production, one needs to know the inclusive fragmentation functions $D_a^A(z, Q^2)$. These functions describe the density of particles of type A at a fractional jet momentum z produced from the hadronization of a parton (-system) a. They may depend on the scale Q^2 of the underlying hard scattering process.

In the present analysis, the LUND fragmentation scheme [8,10] has been utilized to generate the functions $D_a^A(z, Q^2)$ for a = u,d,s,$\bar{u}$,$\bar{d}$,$\bar{s}$,g,(ud) and A = π^+, π^-, K^+, K^-, p, $\bar{p}$. The z distributions given by the LUND model were fitted in the region $0.2 < z < 1.0$ for a fixed jet momentum of 10 GeV/c (which is of the order of the trigger jet momentum) using the empirical analytic shape

$$z \cdot D_a^A(z) = (c_1 + c_2 z + c_3/z) \cdot (1-z)^{c_4} ,$$

c_1, c_2, c_3, c_4 being adjustable parameters. Scale breaking effects were neglected since they are less important for the ratios of cross sections to be calculated. Some typical ud fragmentation functions are shown in fig. 5(a).

Three ingredients of the standard LUND fragmentation scheme were slightly changed:

(a) The strangeness suppression factor p(s)/p(u), where p(q) is the probability to create a $q\bar{q}$ pair in the fragmentation chain, was set to a value of 0.45 (standard value = 0.30) in order to agree with the measured $\sigma(K^+)/\sigma(\pi^+)$ ratio [2].

(b) The probability to create diquark pairs in the fragmentation chain relative to that of quark pair production was fixed at 0.03 (standard value 0.065), in order to fit the $\sigma(\bar{p})/\sigma(\pi^-)$ ratio (figs 1,2 and ref. [1]).

(c) Gluons fragment by splitting into $q\bar{q}$ pairs [8]. The two quarks fragment independently. With this gluon fragmentation the ratio $\sigma(K^-)/\sigma(\pi^-)$ [2] is reproduced.

3.2 Scattering amplitude

The amplitudes for the scattering of quarks and gluons are taken from lowest order QCD calculations [6,11]. The ud diquark scattering amplitudes were factorized into a perturbative and a nonperturbative part. The perturbative part is given by the QCD diagrams for the scattering of a pointlike scalar object S, which has the colour structure of a diquark, i.e. S is treated as a colour antitriplet. The results are given in the appendix. The scattering amplitudes squared $|\Gamma(qS \to qS)|^2$, $|\Gamma(SS \to SS)|^2$, and $|\Gamma(gS \to gS)|^2$ are shown in fig. 5(b) as a function of the scattering angle θ^* in the parton-parton centre-of-mass system and compared with the corresponding amplitudes squared for quark scattering. The main contributions to the high p_T cross section at forward angles $\theta \leq 50°$ come from the angular region $10° < \theta^* < 100°$ in the parton-parton c.m.s. One notices here, that the scattering amplitudes squared for scalar objects are, to a good approximation, identical to those for quark scattering:

$$|\Gamma(qS \to qS)|^2 \sim |\Gamma(SS \to SS)|^2 \sim |\Gamma(q_i q_j \to q_i q_j)|^2$$

$$|\Gamma(gS \to gS)|^2 \sim |\Gamma(gq \to gq)|^2 \ .$$

The nonperturbative part is given by a form-factor $F(Q^2)$ (see below) which describes the inner structure of the diquarks. While

$|\Gamma(qS \to qS)|^2$ and $|\Gamma(gS \to gS)|^2$ are damped by a factor F^2, the diquark-diquark amplitude squared $|\Gamma(SS \to SS)|^2$ is damped by F^4 and is therefore relatively unimportant.

3.3 Structure functions

As proposed in ref. [9] we assume that the proton can be in a state consisting of a single quark and a bound ud diquark system in the isospin and spin ground state I=S=0. Let λ be the probability that a proton is found in this diquark state. Then the proton wave function can be written in the form

$$|p\rangle = \sqrt{1-\lambda}\ |u,u,d,g,sea\rangle + \sqrt{\lambda}\ |\tilde{u},(\tilde{ud}),\tilde{g},\tilde{sea}\rangle$$

(this changes the absolute normalization of the predicted meson cross sections by less than a factor $(1-\lambda)$). The structure of the state $|u,u,d,g,sea\rangle$ is given by a parametrization of the CDHS collaboration [12]; $\tilde{sea}$ = sea is assumed throughout. We constructed three sets of structure functions for the proton in the diquark state. These will be referred to as models 1,2,3(*).

(1) The gluon function is unchanged as compared to the CDHS parametrization. Since only one u valence quark is left in the proton we divide the CDHS structure function u(x) by 2.

$$\tilde{u}(x) = 0.5 \cdot u(x) .$$

Since no valence d quark is left in the proton one has

$$\tilde{d}(x) = 0.$$

The diquark function was then chosen in a way which fulfills the momentum conservation sum rule automatically:

$$(\tilde{ud})(x) = 0.5 \cdot u(x) + d(x).$$

(*) Scaling violations are implicitely obtained through the relations given below, but not mentioned explicitely.

Note that in this model the diquark, which itself is a bound system, does not contain any gluons from the proton.

(2) This model represents the opposite extreme as compared to model 1. All gluons are used for the binding of the diquark:

$$\tilde{u}(x) = 0.5 \cdot u(x)$$

$$\tilde{d}(x) = \tilde{g}(x) = 0$$

$$(\tilde{ud})(x) = 0.5 \cdot u(x) + d(x) + g(x).$$

(3) In models 1 and 2 the probability λ for the diquark state is assumed to be a constant. There are however, experimental [13] and theoretical [14] suggestions that diquarks should appear predominantly at higher Bjorken x values ($x > 0.3$–0.5). Therefore we modify model 2 with the additional assumption

$$\lambda = x.$$

This excludes diquarks at $x = 0$ while the proton is always in the diquark state at $x = 1$.

In all models the structure function d(x) is steeper than u(x) by a factor (1–x) for $x \to 1$ as expected from counting rules [15] and as found by experiments [16].

The effective diquark structure functions $\lambda \cdot (\tilde{ud})(x)$ for the different models are illustrated in fig. 5(c). Integration of these structure functions yields the fractional proton momentum carried by the diquark component: it is ~ 6% in model 1, ~ 13% in model 2 and ~ 13% in model 3.

3.4 Form factor

Since the diquark is an extended object the cross section for diquark scattering is damped by a Q^2 dependent form-factor $F(Q^2)$ [14]. Since only the S=I=0 diquark is taken into account we need to define only

one such factor. As in ref. [9] we use the analytic form

$$F(Q^2) = 1/(1+Q^2/M^2).$$

The scale factor M^2 and the probability λ (in models 1,2) were adjusted such that the predicted normalization and p_T dependence of the ratio $\sigma(p)/\sigma(\pi^+)$ reproduce approximately the data at $\sqrt{s}$ = 62 GeV, $\theta \sim 45°$ and $p_T \sim 4$ GeV/c. The resulting parameters for the models are then:

model 1: $\lambda = 0.30$ $M^2 = 20$ GeV^2/c^4
model 2: $\lambda = 0.17$ $M^2 = 10$ GeV^2/c^4
model 3: $\lambda = x$ $M^2 = 9$ GeV^2/c^4 .

A comment on the numerical values of M obtained in this way is in order here: In the framework of any diquark model the functions $D^P_{ud}(z)$, $(\tilde{ud})(x,Q^2)$ and $F(Q^2/M^2)$ have to be introduced, which depend on different variables, and are rather arbitrary so far. These functions are generally different from the ones entering models for meson production by quark and gluon scattering. Hence one is in a position to construct in a rather natural way e.g. relative proton yields which do depend on $\sqrt{s}$, p_T and θ in contrast to relative meson yields. However, one has to keep in mind that the calculated cross sections depend sensitively on the product $\lambda \cdot D^P_{ud}(z) \cdot (\tilde{ud})(x,Q^2) \cdot F^2(Q^2/M^2)$. This implies that the numerical values of M are influenced by the choice especially of $(\tilde{ud})(x,Q^2)$ and also of λ due to the normalization procedure. A separate evaluation of the shape of the diquark structure function and of the form factor seems to become feasible due to the differential data available now, but is outside the scope of this analysis. We conclude therefore that the parameters M derived here optimize the agreement with the data, but do not necessarily represent a reliable determination of a diquark property.

4. COMPARISON WITH THE DATA

In figs 1,2 and 3 the predictions of the models are compared to the measured p_T, θ and $\sqrt{s}$ dependences of the baryon fractions. The antiproton fractions are in good agreement with all three diquark models

as well as with our standard model ($\lambda = 0$). As expected, the standard model predictions are almost constant in p_T, θ and $\sqrt{s}$ and not much different for proton and antiproton fractions. Thus they are in obvious disagreement with the proton data. The diquark models on the contrary are successful in describing the $\sigma(p)/\sigma(\pi^+)$ ratio (and hence also the $\sigma(p)/\sigma(K^+)$ ratio) at $\theta \sim 45°$. The best prediction of the p_T dependence is achieved by model 3. The measured θ dependence lies between the results from models 1 and 2 while model 3 tends to be too steep in θ. All three models also predict a strong $\sqrt{s}$ dependence of $\sigma(p)/\sigma(\pi^+)$ at $\theta \sim 45°$. The measured slope is well reproduced by model 1, a stronger energy dependence is predicted by models 2,3.

We conclude from these results that:

(a) The trends of the measured proton fractions are in agreement with any of the diquark models.

(b) A more quantitative agreement with the data can be achieved in a model in which the diquark contains only part of the gluon component of the proton.

(c) A more careful analysis of all available data is needed to set restrictive bounds on the shape of the diquark structure function and on the form factor.

Further experimental data are currently being analyzed to establish by independent means the existence of ud diquark scattering. Production of the $\Delta^{++}(1232)$ resonance at high p_T as well as properties of the spectator jets [17] and quantum number correlations in events with a proton of high transverse momentum will be investigated.

5. CONCLUSIONS

The measured relative proton and antiproton yields at high p_T were compared with quantitative model predictions. Standard parton models of quark and gluon scattering combined with commonly used fragmentation

algorithms fail to reproduce the absolute value as well as the p_T, θ, and $\sqrt{s}$ dependence of the proton fractions. Simple models in which ud diquark systems in the proton are allowed to be emitted in a hard process are in reasonable agreement with the data. In the framework of models considered in this paper a situation is preferred in which the ud diquark contains part of the gluon component of the proton.

Acknowledgements

The Dortmund and Heidelberg groups were supported by a grant from the Bundesministerium für Wissenschaft und Forschung of the Federal Republic of Germany. The Ames group was supported by the U.S. Department of Energy under contract W-7405-eng-82.

APPENDIX

The cross sections

$$\frac{d\sigma}{dt} = \pi \frac{\alpha_s^2}{s^2} |\Gamma|^2 = \frac{1}{16\pi s^2} \langle |A|^2 \rangle, \quad \text{where}$$

$\alpha_s = \frac{g^2}{4\pi}$ = strong coupling constant,

s,t,u = Mandelstam variables for the scattering process,

A = invariant QCD amplitudes,

$\langle |A|^2 \rangle = g^4 . |\Gamma|^2$

= amplitudes squared summed and averaged over spins and colours,

for lowest order parton-parton scattering were calculated for the case of pointlike spin 0 colour (anti)triplets S. The calculations are based on the methods described in ref. [11].

The following indices are used throughout:

i,j,m,l = 1-3 (colour triplet indices)

a,b,c = 1-8 (colour octet indices).

(a) The process qS → qS:

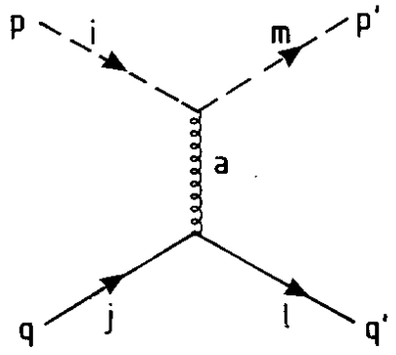

The invariant amplitude reads

$$A(qS \to qS) = -\frac{g^2}{t^2} T^a_{mi} T^a_{j\ell} \cdot (\bar{u}(q')\gamma^\mu u(q)) \cdot (p'+p)_\mu$$

where $T^a_{mi} = \lambda^a_{mi}/2$ are the standard SU(3) matrices (see e.g. ref. [11]). Averaging over initial states of spin and colour and summing over final states gives the result

$$\langle |A(qS \to qS)|^2 \rangle = g^4 \cdot (-\frac{8}{9} \frac{us}{t^2}).$$

(b) The process SS → SS:

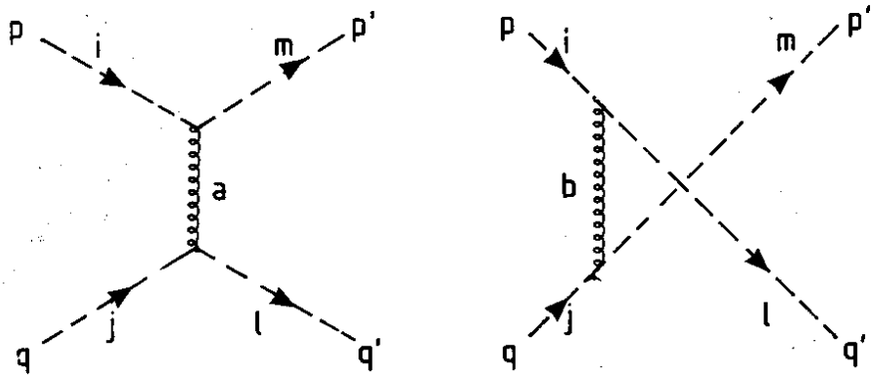

The amplitudes read

$$A_t(SS \to SS) = \frac{g^2}{t} T^a_{mi} T^a_{\ell j} \cdot (p+p')_\mu \cdot (q+q')^\mu$$

$$A_u(SS \to SS) = \frac{g^2}{u} T^b_{\ell i} T^b_{mj} \cdot (p+q')_\nu \cdot (q+p')^\nu .$$

The spin and colour average yields the result

$$\langle |A(SS \to SS)|^2 \rangle = g^4 \frac{2}{9} \cdot \{\frac{(s-u)^2}{t^2} + \frac{(s-t)^2}{u^2} - \frac{2}{3} (1 + \frac{2s^2}{ut})\}$$

(c) The process gS → gS

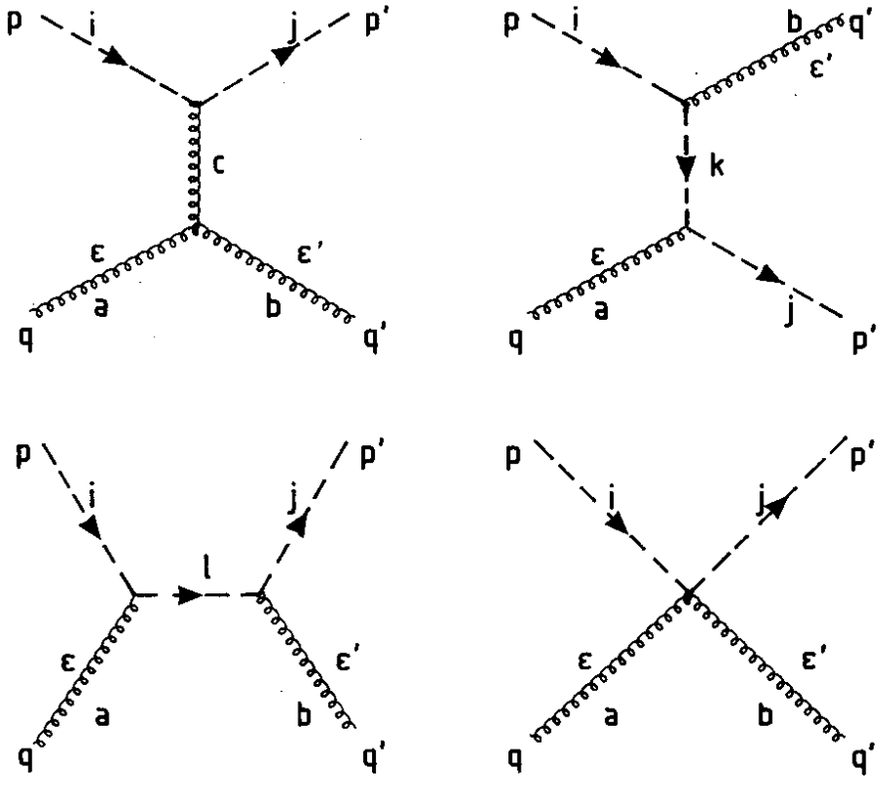

The amplitudes read

$$A_t(gS \to gS) = \frac{g^2}{t} f_{abc} T^c_{ji} \varepsilon^\mu \varepsilon'^\nu C_{\lambda\mu\nu}(q-q',-q,q') \cdot (p+p')^\lambda$$

$$A_u(gS \to gS) = -\frac{ig^2}{u} T^b_{ki} T^a_{jk} \varepsilon^\mu \varepsilon'^\nu \cdot (2p-q')_\nu \cdot (2p'-q)_\mu$$

$$A_s(gS \to gS) = -\frac{ig^2}{s} T^a_{\ell i} T^b_{j\ell} \varepsilon^\mu \varepsilon'^\nu \cdot (2p+q)_\mu \cdot (2p'+q')_\nu$$

$$A_x(gS \to gS) = ig^2 \, \varepsilon^\mu \varepsilon'^\nu \, g_{\mu\nu} \cdot (T^b_{ki} T^a_{jk} + T^a_{ki} T^b_{jk})$$

where ε, ε' are the polarization four vectors of the gluons, f_{abc} are the SU(3) structure constants and $C_{\lambda\mu\nu}$ contains the Lorentz structure of the three gluon coupling:

$$C_{\lambda\mu\nu}(q_1,q_2,q_3) = (q_1-q_2)_\nu g_{\lambda\mu} + (q_2-q_3)_\lambda g_{\mu\nu} + (q_3-q_1)_\mu g_{\nu\lambda}.$$

The spin and colour sums yields

$$\langle |A(gS \to gS)|^2 \rangle = g^4 \cdot \left(\frac{1}{2} \frac{(s-u)^2}{t^2} + \frac{7}{18}\right).$$

REFERENCES

[1] A. Breakstone et al., Phys. Lett. 147B (1984) 237.

[2] A. Breakstone et al., Phys. Lett. 135B (1984) 510.

[3] A. Breakstone et al., Composition of hadrons at large p_T and medium angles in pp, dd, and $\alpha\alpha$ collisions at the ISR, submitted to Phys. C.

[4] D. Antreasyan et al., Phys. Rev. D19 (1979) 764;
H.J. Frisch et al., Phys. Rev. D27 (1983) 1001.

[5] J.J. Aubert et al., Phys. Lett. 135B (1984) 225.

[6] D. Drijard et al., Phys. Lett. 121B (1983) 433;
T. Lohse, Diploma Thesis, University of Dortmund 1982, unpublished.

[7] H.G. Fischer, Proceedings of the Int. Conf. on High Energy Physics, Lisbon, 9-15 July 1981, Ed. J. Dias de Deus, J. Soffer, page 297.

[8] B. Andersson et al., Z. Phys. C13 (1982) 361.

[9] S. Frederiksson et al., Z. Phys. C14 (1982) 35;
S. Frederiksson et al., Z. Phys. C19 (1983) 53;

[10] B. Andersson et al., Nucl. Phys. B197 (1982) 45.

[11] R. Cutler and D. Sivers, Phys. Rev. D16 (1977) 679;
R. Cutler and D. Sivers, Phys. Rev. D17 (1978) 196;
B.L. Combridge et al., Phys. Lett. 70B (1977) 234;
T. Lohse, Ph.D. thesis, Univ. of Dortmund, 1985.

[12] H. Abramowicz et al., Z. Phys. C12 (1982) 289.

[13] F. Eisele, Proceedings of the Int. Conf. on Neutrino Physics and Astrophysics, Maui, Hawaii, 1-8 July 1981, Ed. R.J. Cence, E. Ma, A. Roberts, vol. 1 (1981) p. 297.

[14] I.A. Schmidt and R. Blankenbecler, Phys. Rev. D16 (1977) 1318.

[15] J.F. Owens et al., Phys. Rev. D18 (1978) 1501.

[16] A. Bodek et al., Phys. Rev. D20 (1979) 1471;
D. Allasia et al., Phys. Lett. 135B (1984) 231.

[17] D. Drijard et al., Nucl. Phys. B156 (1979) 309.

FIGURE CAPTIONS

Fig. 1 Particle ratios $\sigma(p)/\sigma(K^+)$, $\sigma(\bar{p})/\sigma(K^-)$ (a) and $\sigma(p)/\sigma(\pi^+)$, $\sigma(\bar{p})/\sigma(\pi^-)$ (b) at $\theta \sim 45°$ as function of p_T. The lines represent the predictions of the models described in the text.

Fig. 2 Angular dependence of R(p) and $R(\bar{p})$ at fixed p_T together with the model predictions.

Fig. 3 $\sqrt{s}$ dependence of $\sigma(p)/\sigma(\pi^+)$ at $x_T = 0.15$ and $\theta \sim 45°$ together with model predictions. Also shown are data from ref. [4] taken at $\theta \sim 90°$.

Fig. 4 R(p) and $R(\bar{p})$ at $x > 0.2$ in deep inelastic muon-nucleon scattering as a function of z together with predictions of the LUND model (both from ref. [5]). Relative (anti) proton yields [1] $\theta \sim 45°$ and $p_T \sim 4$ GeV/c are shown at $z = 0.75$.

Fig. 5 (a) Effective diquark structure functions used in the three diquark models.

(b) Angular dependence of the scattering amplitudes squared for pointlike spin 0 colour antitriplets. For comparison the amplitudes squared for spin 1/2 triplets are also shown.

(c) Analytic approximation to the inclusive fragmentation functions from the LUND model (see text).

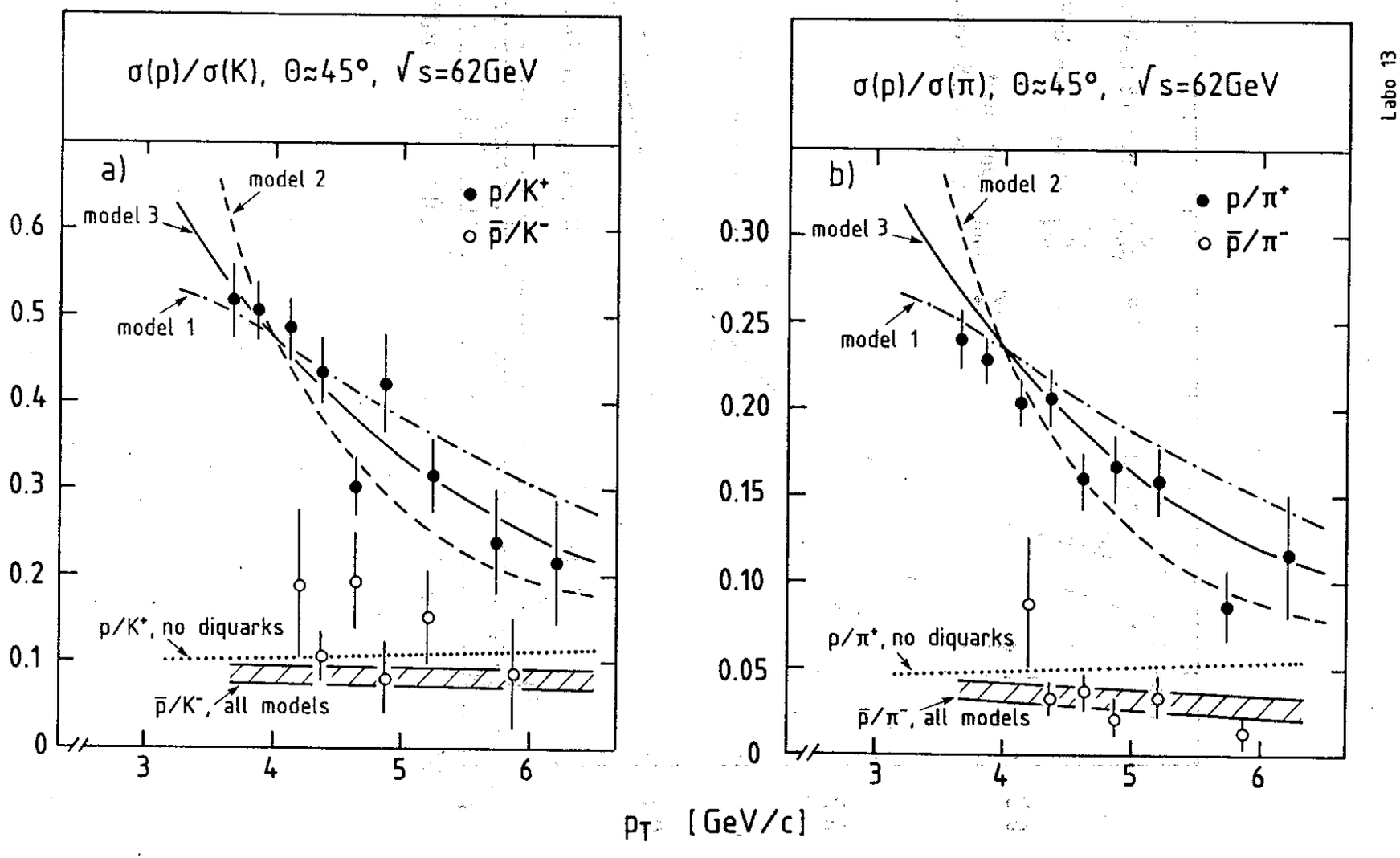
σ(p)/σ(K), θ≈45°, √s=62GeV
a)
model 2
model 3
model 1
p/K⁺
p̄/K⁻
p/K⁺, no diquarks
p̄/K⁻, all models
0.6
0.5
0.4
0.3
0.2
0.1
0
3
4
5
6
σ(p)/σ(π), θ≈45°, √s=62GeV
b)
model 2
model 3
model 1
p/π⁺
p̄/π⁻
p/π⁺, no diquarks
p̄/π⁻, all models
0.30
0.25
0.20
0.15
0.10
0.05
0
3
4
5
6
pT [GeV/c]

Labo 13

Fig. 1

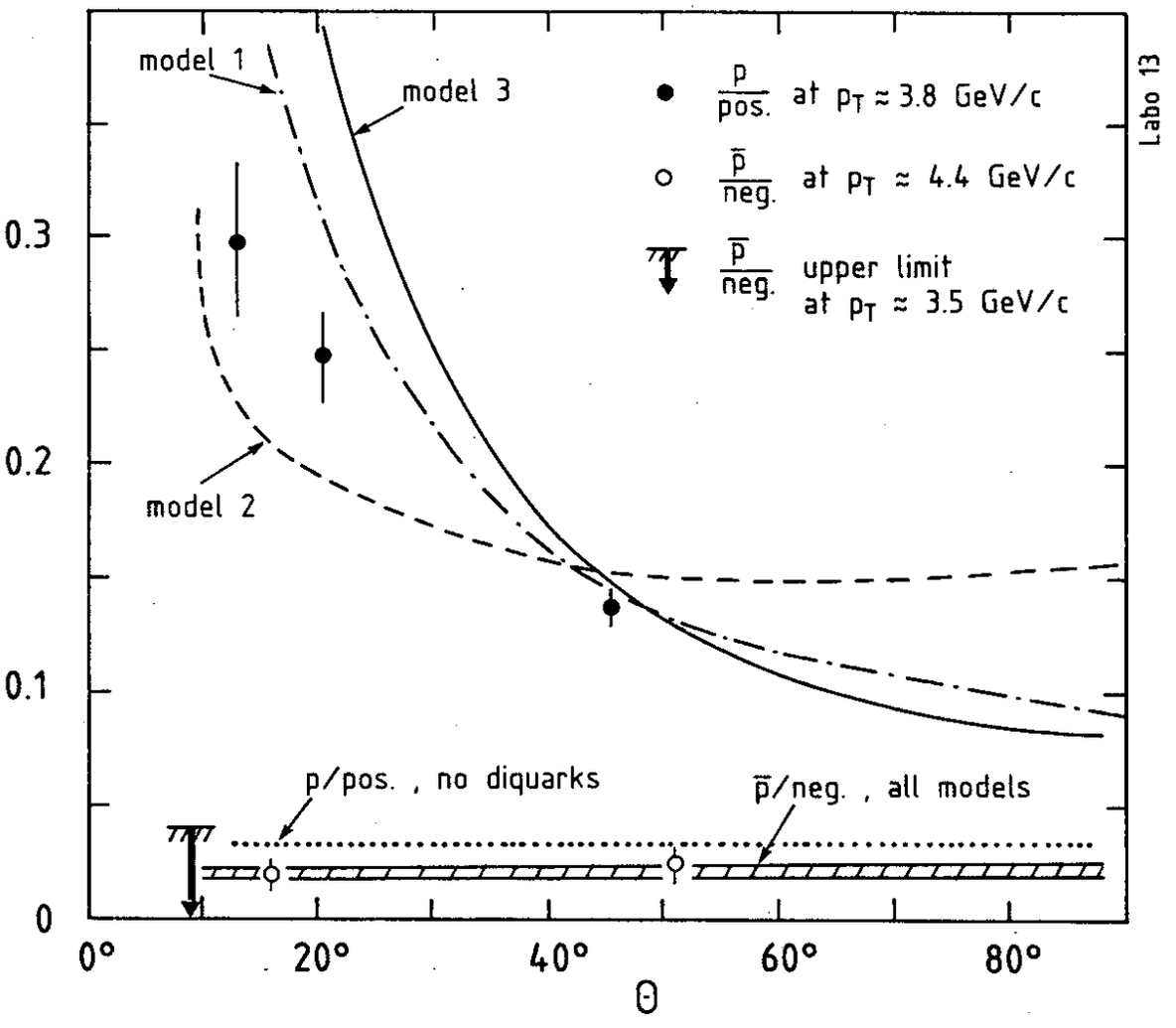
model 1
model 3
model 2
$\frac{p}{pos.}$ at $p_T \approx 3.8$ GeV/c
$\frac{\bar{p}}{neg.}$ at $p_T \approx 4.4$ GeV/c
$\frac{\bar{p}}{neg.}$ upper limit at $p_T \approx 3.5$ GeV/c
p/pos. , no diquarks
$\bar{p}$/neg. , all models
0.3
0.2
0.1
0
0°
20°
40°
60°
80°
Θ
Labo 13

Fig. 2

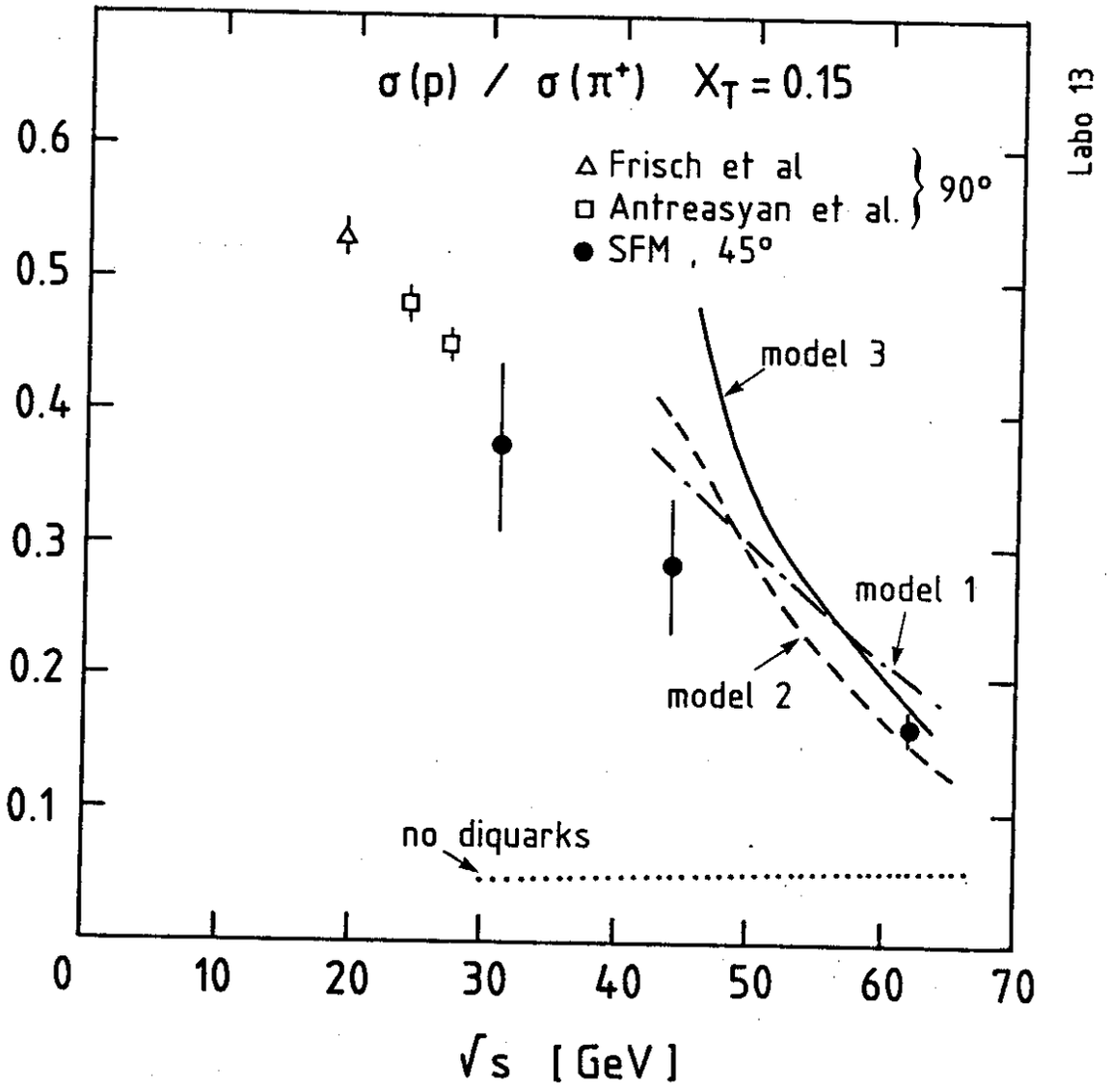
σ(p) / σ(π⁺) X_T = 0.15
Labo 13
Δ Frisch et al
□ Antreasyan et al.
90°
● SFM , 45°
model 3
model 1
model 2
no diquarks
0.6
0.5
0.4
0.3
0.2
0.1
0
10
20
30
40
50
60
70
√s [GeV]

Fig. 3

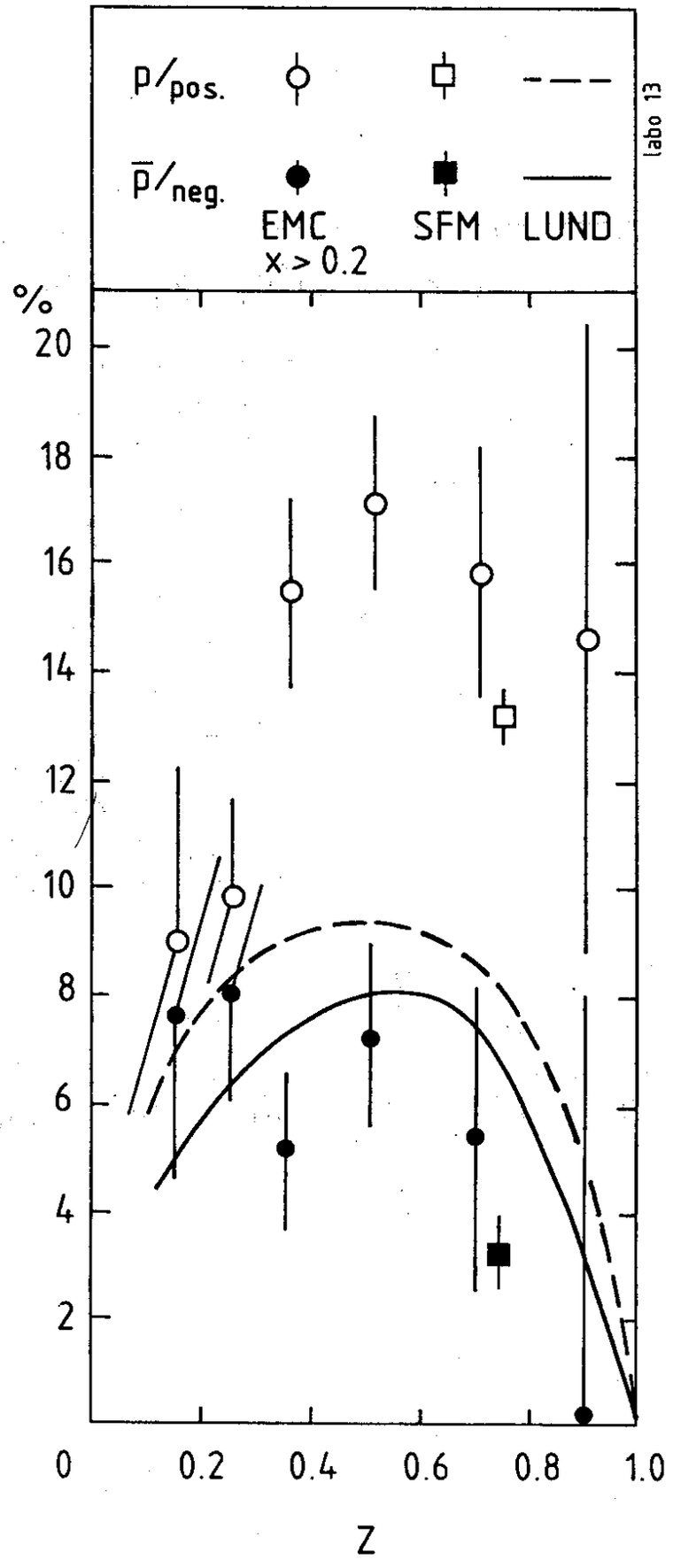
p/pos.
p̄/neg.
EMC
SFM
LUND
x > 0.2
labo 13
%
20
18
16
14
12
10
8
6
4
2
0
0.2
0.4
0.6
0.8
1.0
Z

Fig. 4

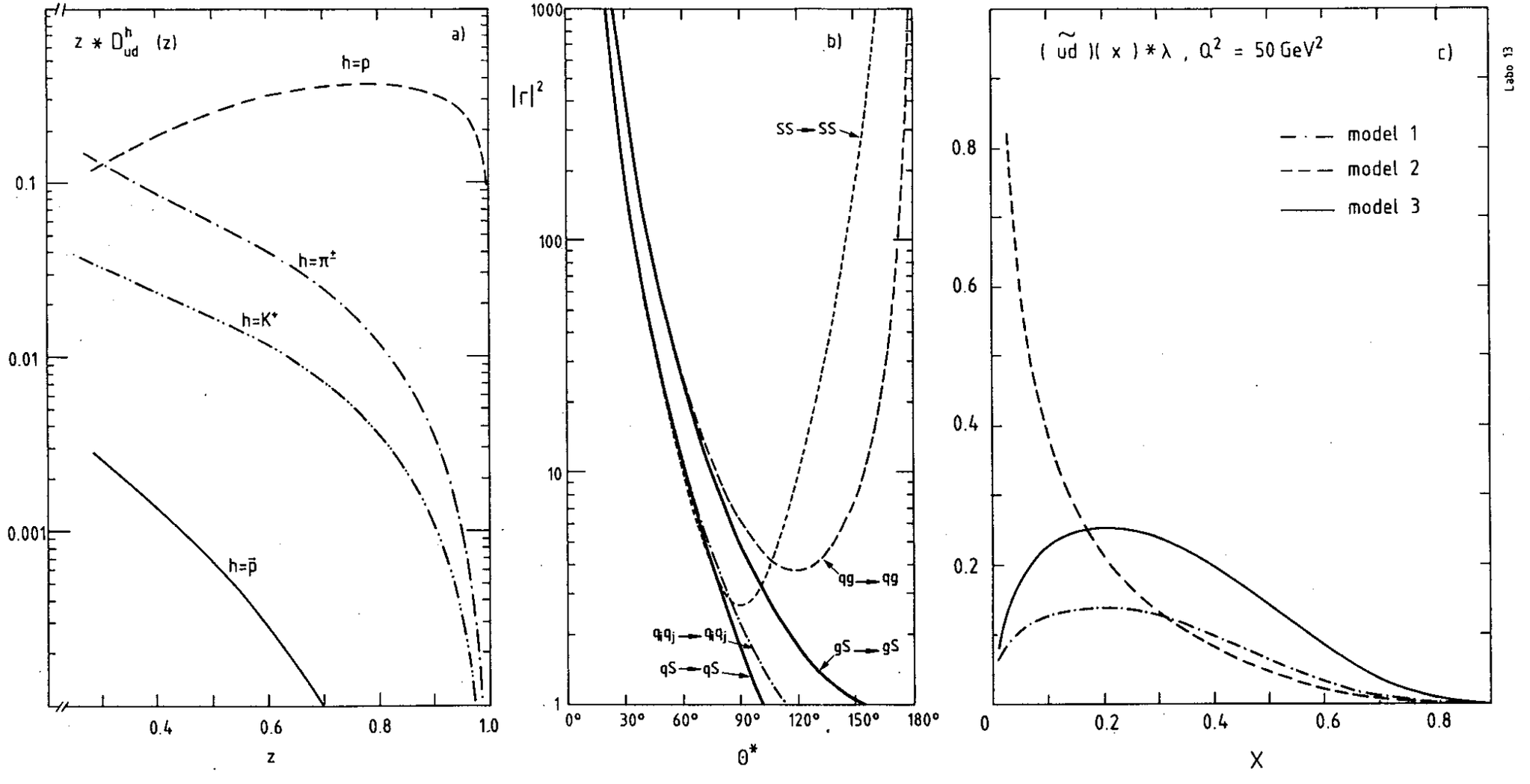
a)
$z * D^h_{ud}$ (z)
h=p
h=π±
h=K±
h=p̄
0.1
0.01
0.001
0.4
0.6
0.8
1.0
z
b)
$|r|^2$
1000
100
10
1
SS → SS
qg → qg
qq_j → qq_j
qS → qS
gS → gS
0°
30°
60°
90°
120°
150°
180°
θ*
c)
(ũd)(x) * λ , Q^2 = 50 GeV²
model 1
model 2
model 3
0.8
0.6
0.4
0.2
0
0.2
0.4
0.6
0.8
X
Labo 13

Fig. 5